Use of a heterogeneous two-dimensional model to improve the primary steam reformer performance

Marisa N. Pedernera, Juliana Piña, Daniel O. Borio, Verónica Bucalá*

Department of Chemical Engineering, PLAPIQUI, Universidad Nacional del Sur, CONICET, Camino La Carrindanga Km 7, 8000 Bahía Blanca, Argentina

Abstract

The reforming units are basically furnaces containing burners (which provide a large amount of heat by fuel combustion) and tubes packed with supported nickel catalyst. Due to the high heat input through the reformer tube wall and the endothermic reforming reactions, the catalyst tubes are exposed to significant axial and radial temperature gradients. For this reason, a two-dimensional mathematical model that takes into account the diffusion reaction phenomena inside the particles rigorously has been used to represent the reactor. Strong radial temperature gradients in the reformer tube have been found, particularly close to the reactor entrance. These temperature differences cause significant variations in the methane reaction rate along the radial position, being the catalyst close to the reforming tube center poorly used. For this reason, the reforming tube diameter and the catalyst activity distribution were modified to use the catalyst more efficiently. The tube diameter has an important influence on the reformer performance, considerable higher conversions and reactor capacities per tube (i.e. closer equilibrium approaches) have been observed for the tubes with smaller diameters. The catalyst activity distribution also strongly impacts the reactor operation. The use of two catalysts of different activity, adequately distributed along the axial and radial directions, allowed to significantly decrease the maximum tube wall temperature and simultaneously minimize the reactor volume fraction packed with the catalyst of higher activity.
© 2003 Elsevier Science B.V. All rights reserved.

Keywords: Steam reforming; Modeling; Two-dimensional heterogeneous model; Catalyst activity distributions

1. Introduction

Steam reforming of hydrocarbons, especially natural gas, is the most important and economic process for production of hydrogen and synthesis gas needed in many chemical and petrochemical processes [1]. The primary reformer is basically a furnace containing burners and tubes packed with a supported nickel catalyst. Due to the strongly endothermic nature of the process, a large amount of heat is supplied by fuel burning (commonly natural gas) in the furnace chamber. Several primary reformer designs are available today, basically they differ in the arrangement of the tubes and the location of the burners in the furnace chamber. These basic designs are classified as top-fired, bottom-fired, side-fired (radiant wall) and terrace wall types [2]. Different firing arrangements result in different tube wall temperatures and heat-flux profiles [3]. For these designs, high heat fluxes are transferred to the catalytic tubes, and therefore the tube skin temperature appears as a key variable. Even a slight increase in the maximum tube wall temperature may result in a serious decline of the expected tube lifetime [4]. Due to the high heat input through the reformer tube wall and the endothermic reforming reactions, the catalyst tubes are exposed to significant axial and radial temperature gradients [3]. For side-fired reformers, axial gas temperature gradients of around 200–270 °C have been reported [5–7]. Regarding to the radial gradients, temperature differences up to 80 °C between the tube wall (internal side) and the centerline were measured for a mono-tube side-fired reformer pilot plant [4]. Primary reformers require two-dimensional models to represent the radial temperature gradients properly, particularly at the tube wall [8].

Pseudo-homogeneous two-dimensional models have been used to simulate the steady-state [4] and non-steady-state [9] operation of catalytic steam reformers. However, the use of pseudo-homogeneous models is not adequate for the representation of primary reformers, since the reactions are strongly diffusion limited with very low effectiveness factors [5,10]. Quinta Ferreira et al. [6], solved a heterogeneous two-dimensional model to simulate a methane steam reformer with large-pore catalysts, considering the strong internal mass-transfer restrictions rigorously. In spite of this,

* Corresponding author. Tel.: +54-291-4861700x265;
fax: +54-291-4861600.
E-mail address: vbucala@plapiqui.edu.ar (V. Bucalá).

Nomenclature

C_{p_k}	heat capacity of component k (kJ/kg K)
d_p	equivalent diameter of the catalyst pellet (momentum equation) (m)
d_{te}	external diameter of the reactor tube (m)
d_{ti}	internal diameter of the reactor tube (m)
D_{er}	effective radial diffusivity (m²/s)
D_k^e	effective diffusivity of component k (m²/s)
f	friction factor
F_k	molar flow rate of component k (kmol/s)
F_t	total molar flow rate (kmol/s)
g	acceleration of gravity (m/s²)
G	superficial mass flow velocity (kg/m² s)
h_p	height of the real catalyst particle (m)
ΔH_i	heat of reaction i, $i = 1, 2, 3$ (kJ/kmol)
M	mean molecular weight (kg/kmol)
Nt	tube number
p_k	partial pressure of component k (gas phase) (bar)
$p_{s,k}$	partial pressure of component k inside the catalyst particle (bar)
p_t	total pressure (bar)
Δp	pressure drop (bar)
Q	heat flux per unit area at axial position z (kW/m²)
r	radial coordinate of the reactor (m)
r_{CH_4}	methane reaction rate (kmol/kg$_{cat}$ s)
$r_{CH_4}^{obs}$	observed methane reaction rate (kmol/kg$_{cat}$ s)
$\bar{r}_{CH_4}^{obs}$	radial mean observed methane reaction rate (kmol/kg$_{cat}$ s)
r^*	dimensionless radial coordinate of the reactor $[r/r_{ti}]$
r_i	rate of the reaction i, $i = 1, 2, 3$ (kmol/kg$_{cat}$ s)
r_{te}	external radius of the reactor tube (m)
r_{ti}	internal radius of the reactor tube (m)
R	universal gas constant (kJ/kmol K)
T	process gas temperature (K)
$\bar{T}$	radial mean temperature (K)
T_{1D}	gas temperature predicted by a one-dimensional model (K)
T_{eq}	equilibrium temperature (K)
T_w	tube skin temperature (K)
$T_{w,max}$	maximum tube skin temperature (K)
u_s	superficial velocity (m³$_f$/m²$_r$ s)
U	overall heat-transfer coefficient (kW/m² K)
V	volume of the catalyst particle (m³)
V_a	volume of the more active catalyst (m³)
V_R	reactor volume (m³)
W	catalyst mass (kg)
x_{CH_4}	methane conversion $[(F_{CH_4}^0 - F_{CH_4})/F_{CH_4}^0]$
x_{CO_2}	conversion of CH$_4$ into CO$_2$ $[(F_{CO_2} - F_{CO_2}^0)/F_{CH_4}^0]$
y_k	molar fraction of component k
z	axial coordinate (m)
z^*	dimensionless axial coordinate (m) $[z/L]$

Greek letters

α_1	activity of the more active catalyst
α_2	activity of the less active catalyst
$\bar{\alpha}$	mean activity defined by Eq. (19)
α_i	convective heat-transfer coefficient (kW/m² K) $[\alpha_i = 8\lambda_{er}\alpha_w/8\lambda_{er} + \alpha_w(r_{ti}/2)]$
α_w	wall heat-transfer coefficient (kW/m² K)
β	reactor volume fraction packed with the catalyst of higher activity
η_i	effectiveness factor for reaction i, $i = 1, 2, 3$
λ_{er}	effective radial thermal conductivity (kW/mK)
λ_t	thermal conductivity of the tube metal (kW/mK)
ξ	radial coordinate of the catalyst particle (m)
ξ^*	dimensionless radius of the equivalent particle $[(\xi - \xi_{in})/(\xi_{eq} - \xi_{in})]$
ξ_{eq}	external radius of the equivalent catalyst particle (m)
ξ_{ext}	external radius of the real catalyst particle (m)
ξ_{in}	hole's radius of the catalyst particle (m)
ρ_B	bed density (kg$_{cat}$/m³$_r$)
ρ_g	gas density (kg/m³$_f$)
ρ_p	density of the catalyst particle (kg$_{cat}$/m³$_{cat}$)

Superscripts

0	at the reactor inlet
s	at the catalyst particle surface

the reforming reactions were represented by a first-order single reaction, therefore the diffusion reaction equation has a simple analytical solution. Currently, there are more accurate kinetics to represent the reforming reactions, particularly the Langmuir–Hinshelwood (Houghen–Watson) type expressions reported by Xu and Froment [12] have been successful in simulating industrial reactors [11].

In this paper, the steady-state operation of large-scale primary reformers is analyzed by means of a heterogeneous two-dimensional model, which accounts for the strong diffusion limitations in the catalyst particle, at each axial and radial reactor position. The kinetic model reported by Xu and Froment [12] is adopted, therefore to evaluate the diffusional resistances the particle mass balances are numerically solved. Particularly, radial methane reaction rates and effectiveness factors are studied in detail. In the present work, the two-dimensional model is also used to compare the steady-state operation of two common industrial reformers (top- and side-fired designs), analyze the influence of the tube diameter on the reformer performance, and study the convenience of using catalyst activity distributions to reduce simultaneously the maximum tube wall temperature and the volume of the catalyst of higher activity.
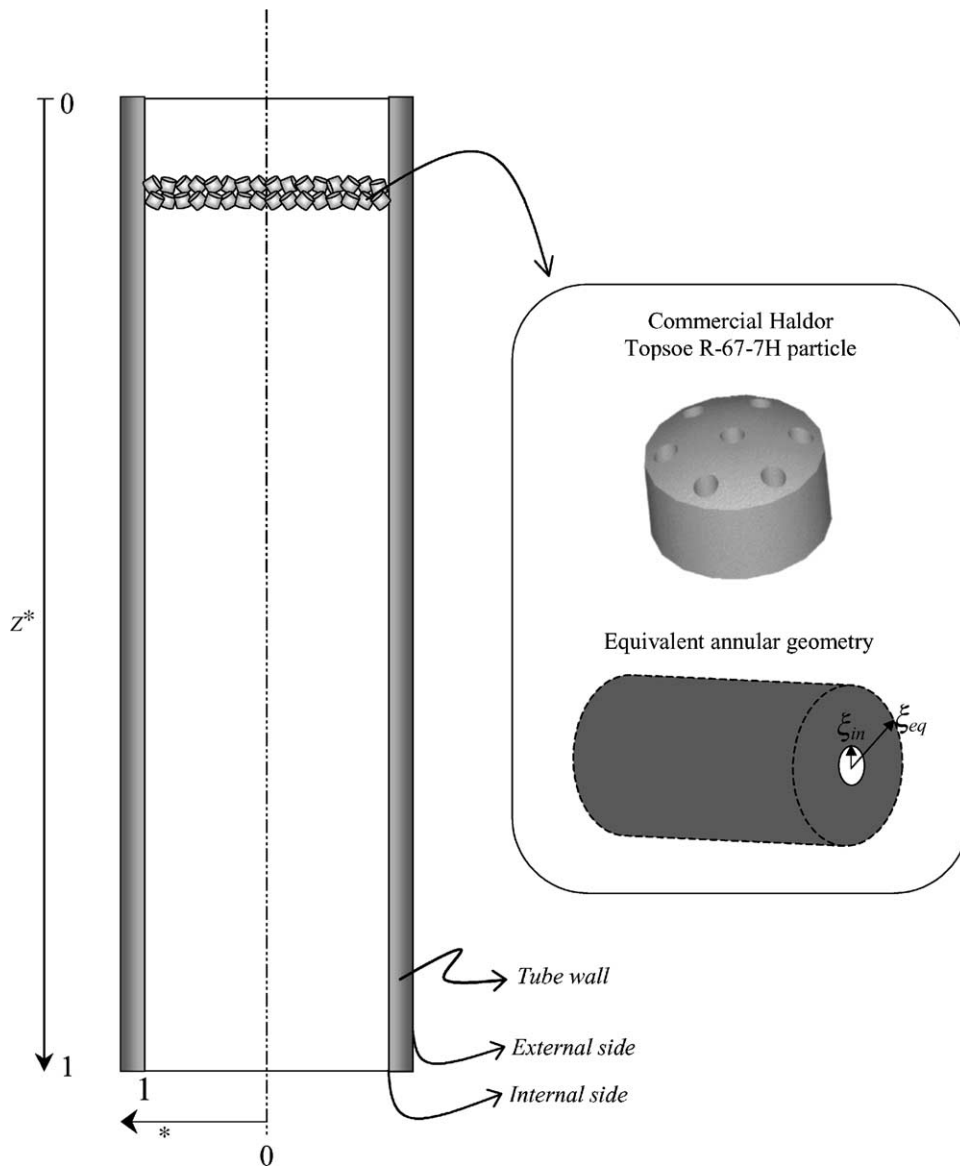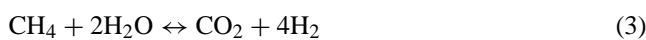
Fig. 1. Schemes of the reformer tube, commercial and equivalent catalyst particles.

2. Mathematical model

The intrinsic kinetic expressions (r_1, r_2 and r_3) reported by Xu and Froment [12] for the steam reforming and water-gas shift reactions are adopted:

$$CH_4 + H_2O \leftrightarrow CO + 3H_2 \tag{1}$$

$$CO + H_2O \leftrightarrow CO_2 + H_2 \tag{2}$$

$$CH_4 + 2H_2O \leftrightarrow CO_2 + 4H_2 \tag{3}$$

To represent the steam reformer, the following assumptions have been considered:

(a) steady-state conditions;
(b) a single reformer tube is representative of any other tube in the furnace;

(c) negligible axial dispersion effects and external mass and heat-transfer resistances;
(d) the catalyst particle is assumed to be isothermal.

For the reforming unit schematically showed in Fig. 1, the governing equations for the bulk and catalyst particle are:

2.1. Gas phase

2.1.1. Mass balances
The mass balance equations are:

$$\frac{\partial x_{CH_4}}{\partial z} = \frac{D_{er}\rho_g}{G}\left[\frac{1}{r}\frac{\partial x_{CH_4}}{\partial r} + \frac{\partial^2 x_{CH_4}}{\partial r^2}\right] + \frac{\rho_B M}{G y_{CH_4}^0}(r_1\eta_1 + r_3\eta_3) \tag{4}$$

$$\frac{\partial x_{CO_2}}{\partial z} = \frac{D_{er}\rho_g}{G}\left[\frac{1}{r}\frac{\partial x_{CO_2}}{\partial r} + \frac{\partial^2 x_{CO_2}}{\partial r^2}\right]$$
$$+ \frac{\rho_B M}{G y_{CH_4}^0}(r_2\eta_2 + r_3\eta_3) \qquad (5)$$

2.1.2. Energy balance

The energy balance equations are:

$$\frac{\partial T}{\partial z} = \frac{M}{G\sum_k y_k Cp_k}$$
$$\times \left[\lambda_{er}\left(\frac{1}{r}\frac{\partial T}{\partial r} + \frac{\partial^2 T}{\partial r^2}\right) + \rho_B\left(\sum_{i=1}^{3}(-\Delta Hr_i)r_i\eta_i\right)\right]$$
$$(6)$$

2.1.3. Momentum equation

The momentum equation is:

$$\frac{dp_t}{dz} = -\frac{f\rho_g u_s^2}{gd_p} \qquad (7)$$

2.1.4. Boundary conditions

At $z = 0$

$$x_{CH_4} = x_{CO_2} = 0; \qquad T = T^0; \qquad p_t = p_t^0 \qquad (8)$$

At $r = 0$

$$\frac{\partial x_{CH_4}}{\partial r} = \frac{\partial x_{CO_2}}{\partial r} = 0 \qquad (9)$$

$$\frac{\partial T}{\partial r} = 0 \qquad (10)$$

At $r = r_{ti}$

$$\frac{\partial x_{CH_4}}{\partial r} = \frac{\partial x_{CO_2}}{\partial r} = 0 \qquad (11)$$

$$\lambda_{er}\frac{\partial T}{\partial r} = U(T_W - T_{r=r_{ti}}) = Q \qquad (12)$$

where

$$\frac{1}{U} = \frac{r_{ti}}{\lambda_t}\ln\left(\frac{r_{te}}{r_{ti}}\right) + \frac{1}{\alpha_W} \qquad (13)$$

2.2. Catalyst particle

The selected catalyst particle (real geometry) is the industrial Haldor Topsoe R-67-7H, table-shaped pellet with convex ends and seven axial holes. Its dimensions, given in the Topsoe Steam Reforming Catalysts R-67 Series Catalogue [13], are included in Table 1. The complex geometry of the real particle is represented by means of an equivalent annular model (see Fig. 1), the internal radius of this representation is supposed to be equal to the radius of the internal holes of the real particle. The external equivalent radius results from considering that the equivalent particle (of infinite length) has the same external surface per unit volume as the real one [14]. The equivalent particle dimensions are also presented

Table 1
Operating conditions and parameters for the simulation of industrial steam reformers

Parameter	Operating conditions
Real catalyst particle	
ρ_p	1990.6 kg_{cat}/m_{cat}^3
ξ_{ext}	0.0083 m
ξ_{in}	0.00158 m
h_p	0.01109 m
Equivalent catalyst particle	
ξ_{eq}	0.002585 m
ξ_{in}	0.00158 m
Reformer tube	
T^0	550 °C
p_t^0	38.7 bar
F_t^0	44.06 kmol/h
$y_{H_2}^0$	2.796%
y_{CO}^0	0.768%
$y_{CO_2}^0$	0.157%
$y_{CH_4}^0$	22.78%
$y_{H_2O}^0$	72.79%
y_{inerts}^0	0.7029%
ρ_B	1016.4 kg_{cat}/m_r^3

in Table 1. The mass balances inside the equivalent particle are as follows:

$$D_{CH_4}^e\frac{1}{\xi}\frac{d}{d\xi}\left(\xi\frac{dp_{s,CH_4}}{d\xi}\right) = RT[r_1(p_{s,j}) + r_3(p_{s,j})]\rho_p \qquad (14)$$

$$D_{CO_2}^e\frac{1}{\xi}\frac{d}{d\xi}\left(\xi\frac{dp_{s,CO_2}}{d\xi}\right) = RT[r_2(p_{s,j}) + r_3(p_{s,j})]\rho_p \qquad (15)$$

2.2.1. Boundary conditions

At $\xi = \xi_{in}$

$$p_{s,CH_4} = p_{CH_4}; \qquad p_{s,CO_2} = p_{CO_2} \qquad (16)$$

At $\xi = \xi_{eq}$

$$\frac{dp_{s,CH_4}}{d\xi} = \frac{dp_{s,CO_2}}{d\xi} = 0 \qquad (17)$$

The wall heat-transfer coefficient (α_w) and the effective radial thermal conductivity (λ_{er}) are estimated using the correlations reported by Dixon and Creswell [15] and Dixon et al. [16]. The effective radial diffusivity (D_{er}) is calculated by means of the expressions given by Froment and Hofmann [17].

The friction factor (*f*) is computed using the equation of Ergun [18]. The equivalent particle diameter for the momentum equation (d_p) is evaluated following the guidelines given by Froment and Bischoff [19].

For the catalyst particle, the values of the effective diffusivities are calculated using the expressions reported by Xu and Froment [5].

2.3. Numerical solution

To solve the system of partial differential equations for the gas-phase, the radial reactor coordinate is discretized by means of central second-order finite differences. The resulting system of ordinary differential equations is integrated using a Gear routine.

The differential equations for the particle (boundary value problem) are discretized by means of second-order finite differences, using an adaptive grid of two elements with variable width. Thirty and 10 grid points are assigned to the first (near the catalyst surface) and the second element, respectively. The 88 resultant non-linear algebraic equations are solved through a quasi-Newton algorithm, for each axial and radial position in the catalyst bed. This allows the calculation of the partial pressure profiles inside the catalyst particle for all the components. The effectiveness factors for reactions (1)–(3) are evaluated as follows:

$$\eta_i = \frac{\int_0^V r_i(p_{s,j}) \frac{dV}{V}}{r_i(p_{s,j}^s)}, \quad i = 1, 2, 3 \tag{18}$$

3. Results and discussion

3.1. Two-dimensional analysis for industrial steam reformers

The two-dimensional model presented in this work provides the temperature and concentration profiles along the reactor radial and axial coordinates and the concentration gradients within the catalyst particle. The side- and top-fired designs are the chosen reformers to be represented by the proposed two-dimensional model, the selected operating conditions corresponding to large-scale units are presented in Table 1. Fig. 2 shows the axial tube wall temperature profiles imposed for both designs. These profiles correspond to those reported by Dybkjaer [20] which are based on measured data from industrial side- and top-fired reformers.

In Fig. 2, the radial mean gas temperature ($\bar{T}$) and the process gas temperature obtained from an equivalent one-dimensional model (T_{1D}) are also displayed for both reformer designs. The one-dimensional model is solved considering the same axial tube skin temperature profiles (T_w) as those used for the two-dimensional model. The convective heat-transfer coefficient for the one-dimensional model (α_i) is calculated using the formula proposed by Froment and Bischoff [19]. The parameters α_w and λ_{er}, which are necessary to estimate the value of α_i, are calculated as it was described for the two-dimensional model. As it can be seen in Fig. 2, the one-dimensional model, although underestimates the gas temperature and the outlet methane conversion, is capable to track the radial mean gas temperature profile. However, the one-dimensional model can not provide information about the strong radial temperature gradients commonly found in the primary reformers. In fact,
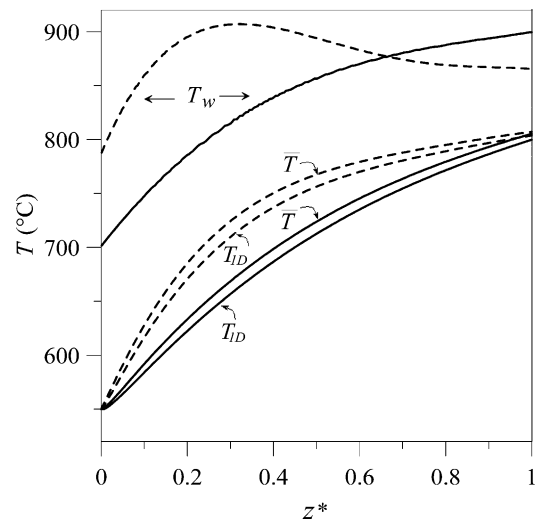

Fig. 2. Tube skin temperature (T_w), radial mean temperature ($\bar{T}$) and temperature predictions given by the one-dimensional model (T_{1D}) as a function of the dimensionless reactor length, for top-fired (dashed lines) and side-fired (solid lines) reformers.

Figs. 3 and 4 show radial temperature gradients (calculated by the two-dimensional model) at three different axial positions in the catalytic tube for the side- and top-fired designs, respectively. The radial mean temperature values are also indicated in Figs. 3 and 4. As it was reported [3], significant radial temperature gradients ($T_{r=r_{ti}} - T_{r=0}$) along the entire reactor length are observed. As a consequence of the higher heat fluxes transferred to the reforming tubes close to the reactor entrance, the top-fired design presents more important radial temperature gradients than the side-fired unit up to approximately $z^* = 0.5$. For both designs, the radial temperature gradients tend to decrease towards the reactor outlet because of the lower local heat fluxes and reforming reaction rates.
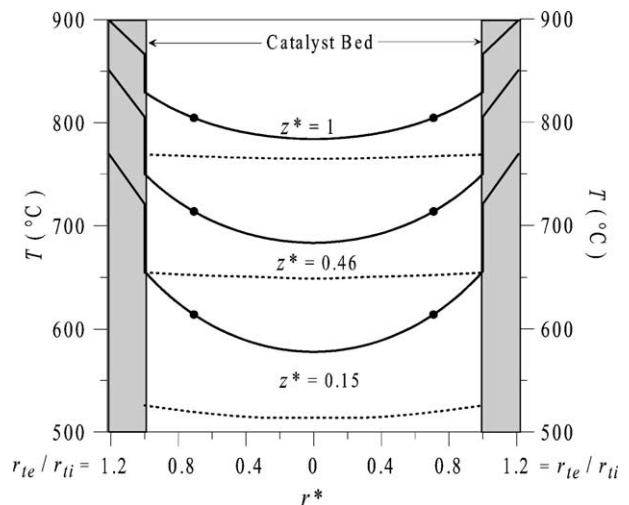

Fig. 3. Side-fired design. Radial temperature gradients in the catalyst tube, for different axial positions (solid lines: wall and gas temperatures; dashed lines: equilibrium temperatures; filled circle: radial mean temperature).
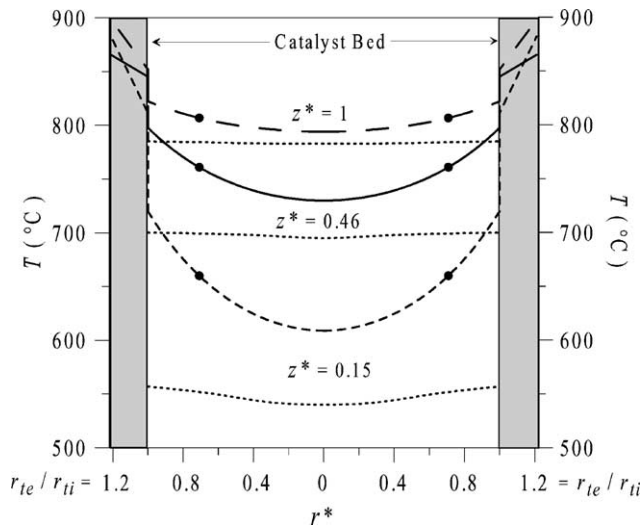
Fig. 4. Top-fired design. Radial temperature gradients for different axial positions (dashed lines: equilibrium temperatures; filled circle: radial mean temperature).
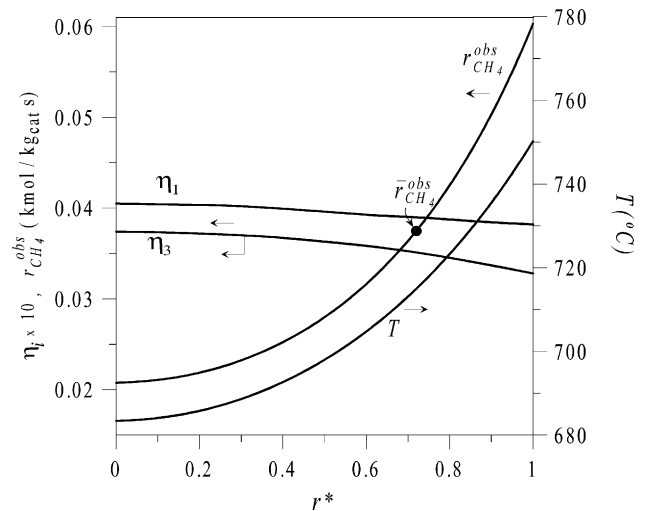

Fig. 5. Observed methane reaction rate, effectiveness factors for reactions (1) and (3), and gas temperature as function of the dimensionless radial coordinate. Axial position $z^* = 0.46$.

Figs. 3 and 4 also include the equilibrium temperatures (T_{eq}). The value T_{eq} is the temperature necessary to attain the same methane conversion level than the one predicted by the two-dimensional model for each radial and axial position, if equilibrium conditions are assumed. The radial gradients for T_{eq} are relatively low, but tend to be higher near the reactor entrance. Due to the important radial mass mixing phenomenon (high flow-rates), mild concentration radial gradients were predicted (by the proposed two-dimensional model) for all the chemical species. However, the calculated slight radial variation of composition tends to be also higher close to the reactor entrance, leading to a difference in T_{eq} of about 20 and 28 °C between the wall and the center of the tube for the side and top designs, respectively. A closer equilibrium approach ($T - T_{eq}$) is observed as the axial coordinate increases, and this approach is maximum at the tube center. At the reactor outlet the radial average temperatures for both designs are similar (Fig. 2), however the equilibrium approach is closer in the case of the top-fired furnace and a higher methane conversion is obtained ($x_{CH_4}^{top} = 0.568$, $x_{CH_4}^{side} = 0.526$). The improvement in the production rates by using a top-fired furnace may be offset by the higher tube mechanical stress due to the presence of greater heat fluxes at axial positions where the tube wall temperatures are high (e.g. $z^* = 0.15$).

Along all the reactor length, the shape of the radial temperature profile and the differences ($T_{r=r_{ti}} - T_{r=0}$) calculated for the side-fired design are similar to those measured from a mono-tube pilot plant reported by Rostrup-Nielsen [3]. Moreover, the observed radial equilibrium approaches ($T(r^*) - T_{eq}(r^*)$) are in good agreement with the data presented by Rostrup-Nielsen et al. [4]. The results given by the proposed two-dimensional model indicate a good capability of the model to follow the operating variables trends observed experimentally.

The proposed two-dimensional model allows to investigate the methane reaction rates, the effectiveness factors and the mass gradients within the catalyst particle along the radial coordinate. For a side-fired reformer, the observed methane reaction rate ($r_{CH_4}^{obs} = \eta_1 r_1 + \eta_3 r_3$) shows an important variation along the radial coordinate (see Fig. 5). Basically, the methane reaction rates follows the trend exhibited by the radial temperature profile because of the relatively flat radial composition profiles. It is important to note that the values of $r_{CH_4}^{obs}$ in the center of the tube are roughly half of the radial mean reaction rate ($\bar{r}_{CH_4}^{obs}$). Consequently, there is a poor utilization of the catalyst portion located near the tube axis. This behavior, described for $z^* = 0.46$ (Fig. 5), was also found for all the axial positions. The significant decrease in the observed reaction rate towards the center of the tube occurs despite of the increase in the effectiveness factors η_1 and η_3 (Fig. 5).

The radial temperature gradients lead to another interesting phenomenon: the inversion of the water-gas shift reaction along the radial direction in the catalyst tube. Fig. 6 shows the curve for the intrinsic reaction rate (r_2^s) at the axial position $z^* = 0.46$. Close to the tube wall the reaction rate at the catalyst surface (r_2^s) changes from positive to negative values. Consequently, the effectiveness factor η_2 presents a discontinuity. Xu and Froment [5], Elnashaie et al. [10], Elnashaie et al. [21], among others, reported an analogous behavior along the axial coordinate of the reactor. The reverse of reaction (2) in the radial coordinate occurs for $z^* \geq 0.4$. For the axial position $z^* = 0.40$ the effectiveness factor discontinuity takes place very close to the reactor wall. However, as the radial mean gas temperature increases along the axial coordinate, the location of this discontinuity is shifted to radial positions closer to the tube center (e.g. at the reactor outlet the reverse of reaction (2) is located at $r^* = 0.5$).
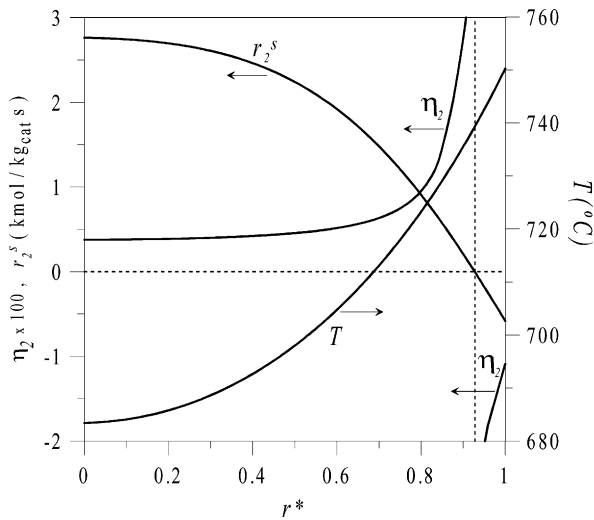
Fig. 6. Intrinsic reaction rate at the catalyst surface, effectiveness factor for reaction (2) and gas temperature as function of the dimensionless radial coordinate. Axial position $z^* = 0.46$.

Due to the strong radial thermal gradients in the reforming tube, the behavior of the catalyst particles is different at each radial position. Figs. 7 and 8 show the methane reaction rate ($r_{CH_4} = r_1 + r_3$) and partial pressure (p_{CH_4}) within the catalyst particle for three different radial positions, respectively. For all the cases the reactions occur in a narrow zone close to the catalyst surface, just about 2.5% of the total depth of the equivalent catalyst particle is being used for the reaction. For the selected conditions, the process gas has reached the equilibrium for $\xi^* > 0.025$ (Figs. 7 and 8). As the radial position in the reactor (r^*) increases towards the tube wall, the temperature, and consequently the reaction rate on the catalyst surface are higher. Thus, a steeper evolution of r_{CH_4} is observed (Fig. 7). For this reason, higher drops in the methane partial concentration are observed near
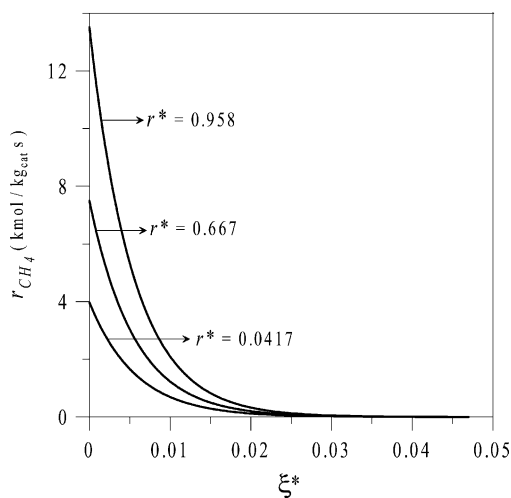

Fig. 7. Methane reaction rate ($r_{CH_4} = r_1 + r_3$) inside the catalyst particle, for three different radial positions in the reformer tube, at the axial position $z^* = 0.46$.
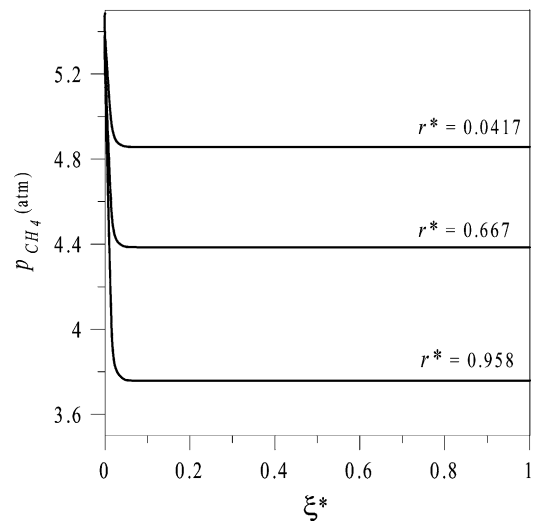

Fig. 8. Methane partial pressure (p_{CH_4}) inside the catalyst particle, for three different radial positions in the reformer tube, at the axial position $z^* = 0.46$.

the tube wall (Fig. 8). The internal gas composition profiles strongly depend on the tube radial position where the catalyst particle is located. In spite of this, for all the axial and radial positions a deficient usage of the catalyst particle is observed.

3.2. Heterogeneous two-dimensional model as a tool to improve the reformer performance

The analysis of industrial reformers by means of the two-dimensional model shows that the methane reaction rate drops significantly near the tube center, because of basically the important radial temperature gradients. This fact indicates that the catalyst located at the center part of the tube is not optimally used. In this work, the reforming tube diameter and the catalyst activity distribution are varied aiming a more efficient usage of the catalyst.

3.2.1. Influence of the tube diameter on the reformer performance

Three different tube diameters have been chosen for this study, the corresponding internal and external diameters are presented in Table 2. The diameters were selected from geometries reported for standard reforming tubes [4]. The behavior of a side-fired reformer has been studied considering that all the tubes sizes are subjected to the same external wall temperature profile, which is shown in Fig. 2. For this

Table 2
Pressure drop and methane conversion for different tube diameters

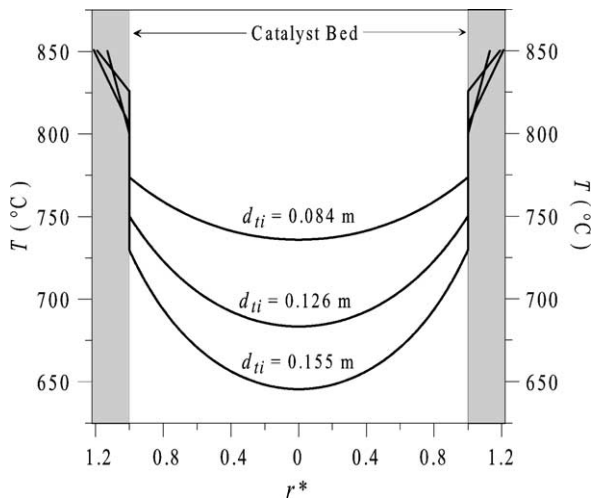| Internal diameter, d_{ti} (m)	External diameter, d_{te} (m)	Methane conversion, x_{CH_4}	Pressure drop, Δp (bar)
0.084	0.100	0.64	5.7
0.126	0.152	0.52	5.2
0.155	0.175	0.48	5.1

Fig. 9. Radial temperature gradients for different internal and external tube diameters at the axial position $z^* = 0.46$.
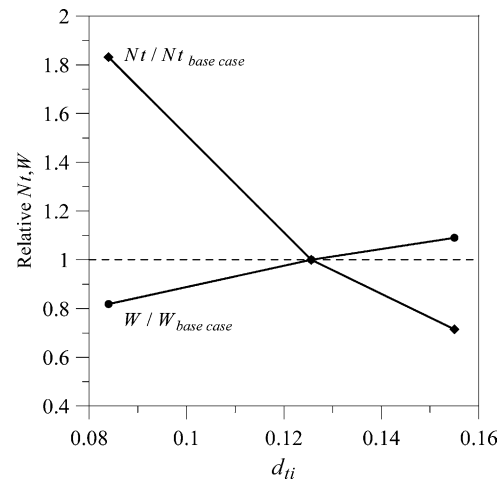

Fig. 10. Influence of the tube diameter on the number of tubes and catalyst mass needed to maintain a given total methane consumption rate. The amounts are relative to the base case ($d_{ti} = 0.126$ m).

analysis, the superficial mass flow velocity (G) has been kept constant for all the tube diameters.

Fig. 9 shows the radial thermal gradients obtained for the axial position $z^* = 0.46$ and for the three tube diameters studied. As the tube diameter diminishes, the radial temperature gradients decrease and the thermal level increases. The higher temperatures and outlet methane conversions (see Table 2) found for the tubes of smaller diameters are due to the higher total heat flux transferred per unit mass of methane fed.

Even though the same superficial mass flow velocity has been selected for all the tube diameters, as it can be seen in Table 2, the pressure drop increases slightly as the diameter diminishes. This behavior is a consequence of the lower gas densities caused by the higher average thermal level found for the smaller diameters (see Fig. 9).

Fig. 10 shows, for the operating conditions of Fig. 9, the relative number of tubes and total catalyst mass required for a given reactor methane consumption rate (i.e. for all the tubes). Smaller tube diameters allow to obtain higher conversions (Table 2) and therefore higher reactor capacities per tube. As a consequence of a more efficient catalyst usage, the total catalyst mass for a given plant capacity diminishes as the tube diameter decreases. However, more tubes are needed to keep the reactor production rate constant. The selection of the reforming tube diameter is a trade-off between, among other variables, the catalyst volume reduction, the slight pressure drop increase and the enlargement of the complex inlet and outlet manifolds caused by a higher number of tubes.

3.2.2. Optimal catalyst activity distribution in the reactor tube

Different catalyst activity distributions are analyzed to improve the reactor operation. For this study, it is assumed that only two catalysts of different activity (α_1 and α_2) are

available to fill the reforming tubes. All the configurations considered are presented in Table 3. The distribution I corresponds to a catalytic bed characterized by a constant mean activity ($\bar{\alpha}$), which is calculated as follows:

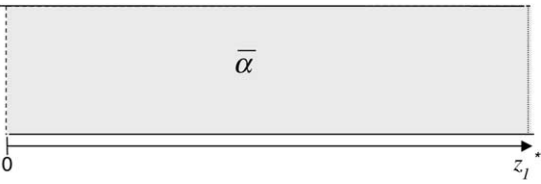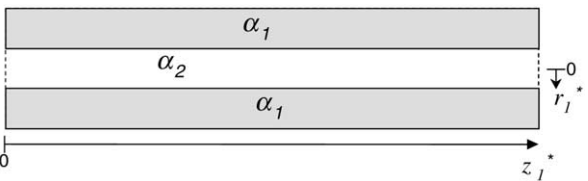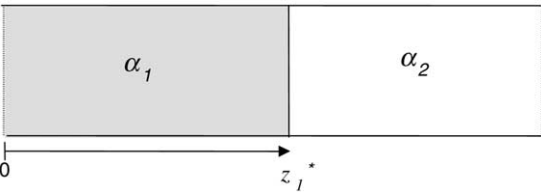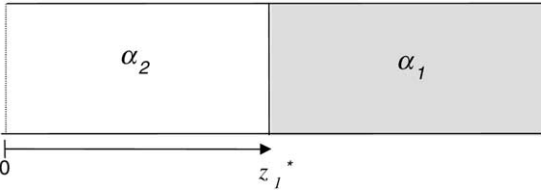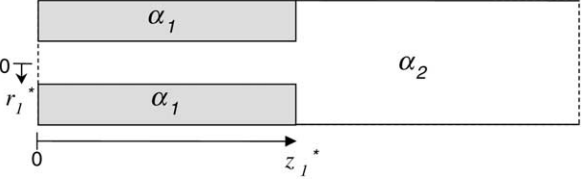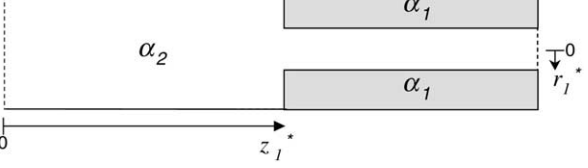$$\bar{\alpha} = \beta\alpha_1 + (1 - \beta)\alpha_2 \qquad (19)$$

where $\beta = V_a/V_R$ represents the reactor volume fraction packed with the catalyst of higher activity (α_1). This activity distribution could be approximately achieved if a volume V_a of a catalyst with activity α_1 is homogeneous mixed (outside the reformer) with a volume ($V_R - V_a$) of the catalyst with a α_2 activity. For the distribution II, the catalyst of higher activity is located in the external annulus of the tube, while the less active catalyst is placed in the tube center. The distributions III and IV represent beds with axial distributions of catalysts of different activity. For the case III, the more active catalyst is located at the reactor entrance (up to z_1^*), while for the curve IV the catalyst particles with higher activity are placed at the end of the reactor (from z_1^* to 1). The cases V and VI are examples of combined axial–radial activity distributions. For all the configurations, the expressions to calculate the reactor volume fraction packed with the catalyst of higher activity (β) are also presented in Table 3.

The influence of the radial and axial distributions of the catalyst activity on the reactor performance is analyzed for the following cases: (a) a deactivated catalyst with an activity of $\alpha_2 = 0.54$ has to be partially or fully replaced with a fresh catalyst ($\alpha_1 = 1$); and (b) the reformer is operating with a standard catalyst ($\alpha_2 = 1$), and the advantage of using a highly active catalyst ($\alpha_1 = 2.2$) has to be evaluated.

3.2.3. Case a: replacement of a deactivated catalyst by a fresh one

A top-fired reformer was selected for this study and for all the catalyst distributions the same heat-flux profile was assumed. The selected heat-flux axial profile corresponds

Table 3
Radial and axial distributions of catalysts of different activity

Distribution	Schematic representation	$\beta = V_a/V_R$
I		
II		$1 - r_1^{*2}$
III		z_1^*
IV		$1 - z_1^*$
V		$z_1^*(1 - r_1^{*2})$
VI		$(1 - z_1^*)(1 - r_1^{*2})$

to that reported by Dybkjaer [20] (average heat flux was 78.5 kW/m²). Fig. 11 shows, for different volume fractions of the more active catalyst, the maximum tube wall temperature calculated for the catalyst distributions I–III and V. The $T_{w,max}$ for $\beta = 0$ corresponds to the maximum tube wall temperature (915.6 °C) obtained with a catalytic bed fully packed with the deactivated catalyst ($\alpha_2 = 0.54$). A reforming tube completely packed with a fresh catalyst ($\alpha_1 = 1$) has a β factor equal to 100%, for this case $T_{w,max}$ is equal to 897 °C. The methane conversion for β equal to 0 and 100% is 52.6 and 53.3%, respectively. The conversions for all the other activity distributions and β fractions, lay between the limits given by the cases of β equal to 0 and 100%.

The complete replacement of the deactivated catalyst causes the maximum tube wall temperature to decrease approximately by 19 °C. This is a well-known phenomenon, however axial and radial distribution can significantly decrease the $T_{w,max}$ value using substantially lower volumes of fresh catalyst.

For all the β values, the annular distribution II leads to maximum tube wall temperatures lower than those obtained with the distribution I. In fact, for the distribution II, the fresh catalyst is located selectively in the radial zones where the methane reaction rate has to be maximized in order to reduce $T_{w,max}$. Although distribution II is an attractive alternative, the axial distribution III is clearly superior for β
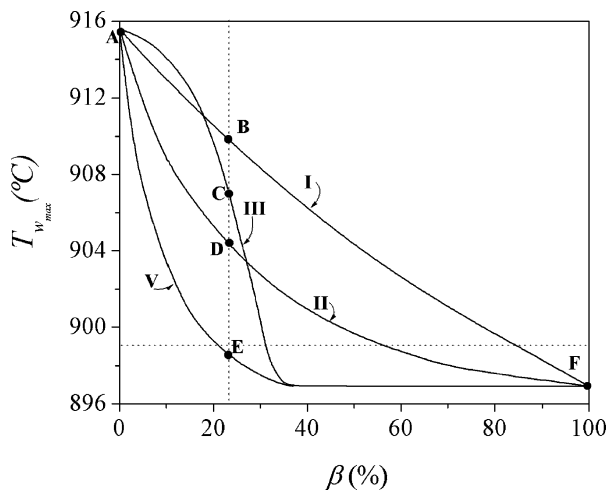
Fig. 11. Maximum tube wall temperature for the activity distributions I–III and V as function of the more active catalyst volume fraction. Top-fired design.

Fig. 12. Tube skin temperature axial profiles for the catalyst activity distributions A–F of Fig. 11.

higher than 37%. Furthermore, using this active catalyst volume ($\beta = 37\%$), the configuration III allows to decrease the $T_{w,max}$ to 897 °C, which is the minimum value achievable in a reactor fully packed with fresh catalyst. The fresh catalyst is more efficiently used by the distribution III, because it is located at the reactor entrance where the maximum tube wall temperature is developed (see Fig. 2). Consequently, for the top-fired designs, the volume of the more active material has to be distributed from the entrance up to an axial position slightly higher than the location of the maximum tube wall temperature.

As it was mentioned, the two-dimensional reformer analysis indicates that the reaction rates are low in the tube center and that the $T_{w,max}$ for the top-fired reformer is located in the first third of the reactor. Therefore, an activity distribution capable to consider both essential characteristics of the reformer should be the best one. For this reason, the distribution V with a fixed value of $z_1^* = 0.37$ and a variable r_1^* was also tested. As it can be seen in Fig. 11, for all the β values the distribution V leads to lower $T_{w,max}$ than the configurations I–III. Moreover, the distribution V allows to obtain the same $T_{w,max}$ by using the lowest active volume. For example, for a maximum tube wall temperature of around 899 °C, the required volume of the more active catalyst for the distributions I–III and V are 82.5, 56.5, 30.5 and 23.4%, respectively. The distributions IV and VI are not convenient for top-fired designs, in fact the active volume is not located in the axial positions where the maximum tube wall temperature takes place.

Fig. 12 shows the axial tube wall temperature profiles obtained for the catalyst activity distributions A–F of Fig. 11. For the cases B–E the same volume of the more active catalyst is used (i.e. $\beta = 23.4\%$). The sudden variations in the slopes of the curves for the cases C and E occur at the axial positions where a discontinuity in the catalyst activity takes place. For $\beta = 23.4\%$, the distribution III (point C of
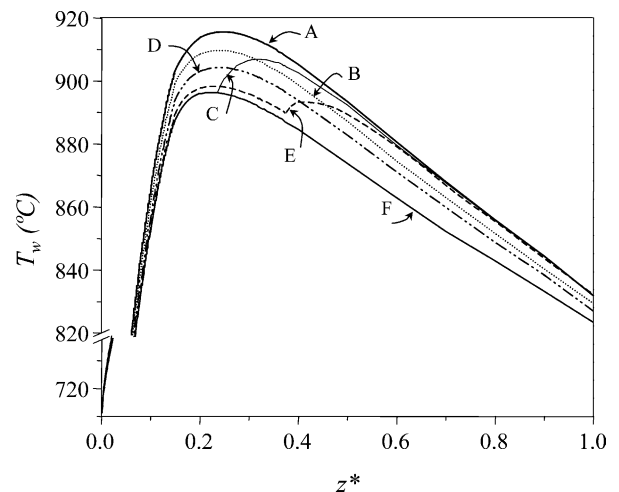
Fig. 11; $z_1^* = 0.234$) is not effective because the more active catalyst is not located at the position of the highest tube wall temperature. However, for the axial–radial distribution V (point E of Fig. 11) the same amount of fresh catalyst (23.4%) is distributed in an annular way up to $z_1^* = 0.37$, being this axial position beyond the location of $T_{w,max}$. In other words, a given mass of the more active catalyst can be more efficiently used by adopting the distribution V. The replacement of 23.4% of the deactivated catalyst by a fresh one and selecting the distribution V ($z_1^* = 0.37$) leads to a $T_{w,max}$ ($\sim$899 °C) just 2 °C higher than the minimum attainable one (i.e. 897 °C for $\beta = 100\%$).

The *case a* was also analyzed for a side-fired reformer. Since for this type of units the $T_{w,max}$ takes place at the reactor outlet, the best replacement of the deactivated catalyst by a fresh one was provided by the activity distribution VI.

3.2.4. Case b: use of a highly active catalyst

This case is illustrated for a side-fired reformer. For this analysis and for all the studied activity distributions, also a given axial heat-flux profile (average heat flux: 90.6 kW/m²) has been selected [20]. Fig. 13 shows the maximum tube wall temperatures calculated for the activity distributions I, II, IV and VI. For a bed fully packed with a standard catalyst ($\alpha_2 = 1$), the $T_{w,max}$ calculated is 922.5 °C (see $T_{w,max}$ for $\beta = 0$). The total replacement of the standard catalyst by a highly active one ($\alpha_1 = 2.2$) causes a $T_{w,max}$ decrease of about 18.3 °C (see $T_{w,max}$ for $\beta = 100\%$). The conversions for all the activity distributions and β fractions vary between 57.4 and 58.6%, which are the methane conversions for β equal to 0 and 100%, respectively. Fig. 13 also shows that the configuration VI (for a fixed value $z_1^* = 0.5$) clearly becomes the best alternative to simultaneously reduce the $T_{w,max}$ value and the mass of the highly active catalyst. For example, if a $T_{w,max}$ of 906 °C is selected, this temperature value can be attainable using 26, 47, 52 and 82% of the
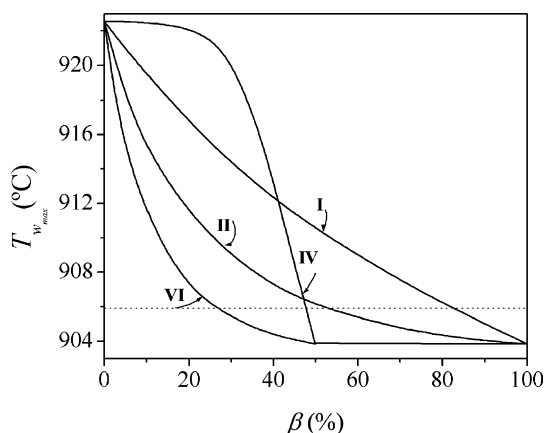
Fig. 13. Maximum tube wall temperature for the activity distributions I, II, IV and VI as function of the more active catalyst volume fraction. Side-fired design.

reactor volume packed with the highly active material for the distributions VI, IV, II and I, respectively.

For this case of study, the radial–axial distribution (i.e. configuration V) also allows to reduce simultaneously the $T_{w,max}$ and the β values for a top-fired reformer.

The combined radial–axial activity distribution offers more significant advantages for the side-fired than for the top-fired reformers.

Even though the proposed radial catalyst distributions would be difficult to be implemented in industrial practice for β values close to 0 and 100% (few catalyst particles can be located across the reformer tube diameter), the annular configurations II, V and IV are feasible for the range of intermediate β values.

4. Conclusions

The radial methane reaction rates, for the side- and top-fired reformers strongly decrease from the tube wall towards the reforming tube center. Because of the negligible radial concentration gradients, the radial reaction rate profiles are basically determined by the radial temperatures.

It is well known that the water-gas shift reaction rate (reaction (2)) reverses its direction at a finite axial position. In the present work, the same phenomenon has been detected in the radial direction for the second half of the reforming tube. The radial coordinate, where reaction (2) reverses, changes from the tube wall towards the tube center as the axial position and the gas temperature increase.

For the two studied reformer designs, the radial temperature gradients are more significant close to the reactor entrance. This effect is particularly remarkable for the top-fired design, which presents higher local heat fluxes near the reactor entrance. For both designs and all the axial positions, the equilibrium approach is closer towards the tube center.

The strong radial variation found for the methane reaction rate indicate that the catalyst located near the tube axis represents a poor contribution to the overall production rate. For this reason, the tube diameter and the catalyst activity distribution have significant influence on the reactor performance. For a given superficial mass flow velocity, as the tube diameter decreases the conversion and reactor capacity increase. The combined radial–axial catalyst distributions (configurations V and VI) allow to significantly decrease the maximum tube wall temperature and simultaneously minimize the mass of the catalyst of higher activity. The convenience of using the combined axial–radial activity distributions were confirmed for different activity levels and for the side- and top-fired reformers.

The proposed two-dimensional model is a useful tool to identify zones in the catalyst bed and within the catalyst particle that are poorly used and propose improvements to obtain a more efficient use of the catalyst.

References

[1] A.M. Adris, B.B. Pruden, C.J. Lim, J.R. Grace, On the reported attempts to radically improve the performance of the steam reforming reactor, Can. J. Chem. Eng. 74 (1996) 177.

[2] S. Lee, Methane and its Derivatives, Marcel Dekker, New York, 1997.

[3] J.R. Rostrup-Nielsen, Catalytic steam reforming, in: J.R. Anderson, M. Boudard (Eds.), Catalysis Science and Technology, vol. 4, Springer, Berlin, 1984, p. 11.

[4] J.R. Rostrup-Nielsen, L.J. Christiansen, J.H. Bak Hansen, Activity of steam reforming catalysts: role and assessment, Appl. Catal. 43 (1988) 287.

[5] J. Xu, G.F. Froment, Methane steam reforming. II. Diffusional limitations and reactor simulation, AIChE J. 35 (1989) 97.

[6] R.M. Quinta Ferreira, M.M. Marques, M.F. Babo, A.E. Rodrigues, Modeling of the methane steam reforming reactor with large-pore catalyst, Chem. Eng. Sci. 47 (1992) 2909.

[7] J.K. Rajesh, S.K. Gupta, G.P. Rangaiah, A.K. Ray, Multiobjective optimization of steam reforming performance using genetic algorithm, Ind. Eng. Chem. Res. 39 (2000) 706.

[8] J.R. Rostrup-Nielsen, Production of synthesis gas, Catal. Today 18 (1993) 305.

[9] H.M. Kvamsdal, H.F. Svendsen, T. Hertzberg, O. Olsvik, Dynamic simulation and optimization of a catalytic steam reformer, Chem. Eng. Sci. 54 (1999) 2697.

[10] S.S.E.H. Elnashaie, A.M. Adris, M.A. Soliman, A.S. Al-Ubaid, Digital simulation of industrial steam reformers for natural gas using heterogeneous models, Can. J. Chem. Eng. 70 (1992) 786.

[11] S.S.E.H. Elnashaie, S.S. Elshishini, Modeling, Simulation and Optimization of Industrial Catalytic Fixed Bed Reactors, Gordon and Breach, Amsterdam, The Netherlands, 1993.

[12] J. Xu, G.F. Froment, Methane steam reforming, methanation and water-gas shift. I. Intrinsic kinetics, AIChE J. 35 (1989) 88.

[13] Topsoe Steam Reforming Catalysts R-67 Series Catalogue, Haldor Topsoe A/S, 1998.

[14] J. Piña, N.S. Schbib, V. Bucalá, D.O. Borio, Influence of the heat-flux profiles on the operation of primary steam reformers, Ind. Chem. Eng. Res. 40 (23) (2001) 5215.

[15] A.G. Dixon, D.L. Creswell, AIChE J. 25 (4) (1979) 663.

[16] A.G. Dixon, A. DiConstanzo, B.A. Soucy, Int. J. Heat Mass Transfer 27 (1984) 1701.

[17] G.F. Froment, P.K. Hofmann, Design of fixed-bed gas-solid catalytic reactor, in: Chemical Reactor and Reactor Engineering, Marcel Dekker, New York, 1987.

[18] S. Ergun, Fluid flow through packed columns, Chem. Eng. Prog. 48 (2) (1952) 89.

[19] G.F. Froment, K.B. Bischoff, Chemical Reactor Analysis and Design, Wiley, New York, 1979.

[20] J. Dybkjaer, Tubular reforming and autothermal reforming of natural gas—an overview of available processes, Fuel Process. Technol. 45 (1995) 85.

[21] S.S.E.H. Elnashaie, M.A. Soliman, M.E. Abashar, S. Almuhana, Mathematical modeling of diffusion and reaction for gas–solid catalytic systems with complex reaction networks. Negative effectiveness factors, Math. Comput. Model. 16 (1992) 41.